Inorganic Chemistry

Article

pubs.acs.org/IC

Light-Driven Hydrogen Production from Aqueous Protons using Molybdenum Catalysts

William T. Eckenhoff,* William W. Brennessel, and Richard Eisenberg*

Department of Chemistry, University of Rochester, Rochester, New York 14627, United States

Supporting Information

ABSTRACT: Homogeneous light-driven systems employing molecular molybdenum catalysts for hydrogen production are described. The specific Mo complexes studied are six-coordinate bis(benzenedithiolate) derivatives having two additional isocyanide or phosphine ligands to complete the coordination sphere. Each of the complexes possesses a trigonal prismatic coordination geometry. The complexes were investigated as proton reduction catalysts in the presence of $[Ru(bpy)_3]^{2+}$, ascorbic acid, and visible light. Over 500 TON are obtained over 24 h. Electrocatalysis occurs between the Mo^{IV}/Mo^{III} and Mo^{III}/Mo^{II} redox couples, around 1.0 V vs SCE. Mechanistic studies by ^1H NMR spectroscopy show that upon two-electron reduction the $Mo(CNR)_2(bdt)_2$ complex dissociates the isocyanide ligands, followed by addition of acid to result in the formation of molecular hydrogen and the $Mo(bdt)_2$ complex.

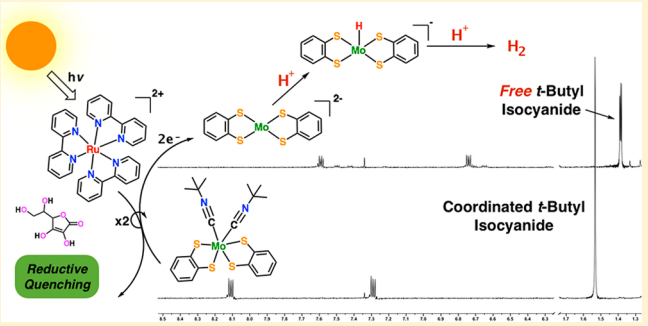

INTRODUCTION

Splitting water into its constituent elements by means of solar radiation for the purpose of energy storage, also known as artificial photosynthesis, marks one of the great challenges for the 21st century.[1−4] Research on the overall process is often divided into its two half-reactions, water oxidation and proton reduction, for convenience of research. Early work in the area of proton reduction relied on the use of rare metal catalysts, such as platinum and palladium colloids, due to their low overpotentials for proton reduction.[5−8] Recent efforts have shown that a number of well-defined complexes composed of earth-abundant metals such as cobalt,[9−19] nickel,[20−26] and iron[27−31] have high activity in aqueous proton reduction systems.[32−35] For purely homogeneous systems, cobalt bis-dithiolene complexes exhibit exceptionally high rates of hydrogen generation as well as total turnover numbers (TON), ranging from 2000 to 9000 depending on the specific complex.[19] This work was a departure from commonly used cobalt diglyoximate complexes, which were shown to suffer from ligand dissociation, leading to complex destruction and limiting their durability and potential long-term activity.[36] However, cobalt bis-dithiolene complexes also suffered from a lack of durability, albeit with much higher turnover frequencies. Part of this higher activity was proposed to result from the noninnocent properties of dithiolene ligands that allowed direct participation of the ligand in the proton reduction mechanism. Calculations of cobalt bis-dithiolene reduction potentials and pK_a's have given insight into mechanistic speculation.[37] Following initial reduction of the complex, the ligating sulfur atoms are thought to be protonated, allowing the second reduction to occur at a more positive potential and therefore to be more thermodynamically favorable. The second reduction is proposed to lead to the generation of a highly reactive cobalt hydride. Intramolecular coupling of the hydride and a proton on a nearby sulfur donor then yields H_2 (a heterocoupling reaction step) and the starting complex. The placement of proton acceptors, such as thiolates, in close proximity to the metal center likely increases the rate at which the final coupling step to form H_2 occurs. This has been shown for other systems with carboxylic acid[38,39] and amine functionalities.[20,22,23] Dithiolene ligands have also been used as bridging ligands in place of 2-aza-1,3-propanedithiolates in diiron hydrogenase model complexes that have also been investigated for proton reduction. In these systems, the notion of ligand protonation has been supported as an integral part of the catalysis.[40,41]

Among heterogeneous proton reduction catalysts, MoS_2 and WS_2 deposited on SiO_2 have been reported to be active in light-driven systems for hydrogen generation using CdS/SiO_2 or fluorescein as photosensitizers over 2 decades ago.[42,43] These initial results showed that WS_2 and MoS_2 materials were competitive in hydrogen production activity with that of similar Pt-based materials. Under UV irradiation, this was also accomplished with MoS_4^{2-} or $[MoS_4(S_2C_2H_4)_2]^{2-}$ supported on TiO_2 nanoparticles.[44] Over the past few years, electrocatalytic materials based on MoS_2 and MoS_3,[45,46] Mo boride and carbide,[45,47] bioderived soy protein materials containing redox active Mo centers,[48] and MoS_x films[49,50] have all been described for this purpose. Reports of highly active photochemical systems using supported MoS_2 nanoparticles as catalysts have also recently come to light.[51−54]

Received: June 20, 2014
Published: August 27, 2014

   dx.doi.org/10.1021/ic501440a | Inorg. Chem. 2014, 53, 9860−9869

With regard to homogeneous molybdenum catalysts for hydrogen generation, both $(CpMo)_2(\mu\text{-}S)_2(\mu\text{-}S_2CH_2)$ (Cp = cyclopentadienyl) and polypyridyl molybdenum complexes have been found to be active as electrochemical hydrogen evolution catalysts.[55−57] However, molybdenum complexes have not yet been reported as active homogeneous catalysts for proton reduction in light-driven systems.

Since MoS_x centers showed great promise for proton reduction chemistry, we conjectured that Mo dithiolene complexes that can be tuned electronically may exhibit similar activity. Neutral molybdenum tris-dithiolene complexes have long been known to possess trigonal prismatic coordination,[58−60] mimicking the Mo coordination found in MoS_2.[61] Since active sites in MoS_2 for hydrogen formation are likely at edges or steps of the solid with a reduced coordination number, we commenced this work focusing on molybdenum bis-dithiolene complexes as possible H_2 generating catalysts. In this article, we describe these studies.

EXPERIMENTAL SECTION

Materials and Methods. All solvents and ascorbic acid were purchased from Fisher Scientific and used without further purification. Benzene-1,2-dithiol (bdt), toluene-3,4-dithiol (tdt), 3,6-chloro-benzene-1,2-dithiol (bdt-Cl_2), *tert*-butylisocyanide (*t*-BuNC), 4-methoxyphenyl-isocyanide (MeOPhNC), benzylisocyanide (BzNC), *n*-butyllithium (*n*-BuLi), methyldiphenylphosphine (PPh_2Me), diphenylphosphinoethane (dppe), sodium amalgam, and $[Ru(bpy)_3]Cl_2$ were purchased from Sigma-Aldrich and used as received. NMR solvents (CD_2Cl_2, D_2O, and CD_3CN) were purchased from Cambridge Isotopes and were employed using residual ^1H resonances at 5.31, 4.79, and 1.94 ppm, respectively.

All NMR spectra were collected on a Bruker 400 MHz NMR spectrometer and processed using iNMR. UV−vis spectra were collected on an Agilent Cary 60. Electrochemical measurements were performed using a CH Instruments 620D potentiostat equipped with a 680C amp booster. Fluorescence quenching was performed on a Jobin Yvon Horiba Fluoromax-P fluorimeter with a photomultiplier tube detector. pH measurements were performed on a model 420 ThermoOrion pH meter.

Single-Crystal X-ray Crystallography. Crystals were placed onto the tips of glass fibers and mounted on a Bruker SMART CCD platform diffractometer for data collection.[62] For each crystal, a preliminary set of cell constants and an orientation matrix were calculated from reflections harvested from three orthogonal wedges of reciprocal space. Full data collections were carried out using Mo Kα radiation (0.71073 Å, graphite monochromator) with frame times ranging from 30 to 60 s and at a detector distance of approximately 4 cm. Randomly oriented regions of reciprocal space were surveyed: four to six major sections of frames were collected with 0.50° steps in ω at four to six different φ settings and a detector position of −38° in 2θ. The intensity data were corrected for absorption.[63] Final cell constants were calculated from the *xyz* centroids of approximately 4000 strong reflections from the actual data collections after integration.[64]

Structures were solved using SIR97[65] and refined using SHELXL-97.[66] Space groups were determined on the basis of systematic absences, intensity statistics, or both. Direct-methods solutions were calculated, which provided most non-hydrogen atoms from the E-map. Full-matrix least-squares/difference Fourier cycles were performed, which located the remaining non-hydrogen atoms. All non-hydrogen atoms were refined with anisotropic displacement parameters. All hydrogen atoms were placed in ideal positions and refined as riding atoms with relative isotropic displacement parameters. Full matrix least-squares refinements on F^2 were run to convergence.

In structures **1**, **2**, **5**, and **6**, each asymmetric unit contains one molybdenum molecule in a general position. For **6**, the asymmetric unit also contains one cocrystallized dichloromethane solvent molecule, which is modeled as disordered over four positions (38:25:24:13). The molybdenum atom of **3** lies on a crystallographic *m*2*m* position and thus one-quarter of the molybdenum molecule is unique. Additionally one *tert*-butyl group is modeled as doubly disordered over two general positions (57:43) and over a crystallographic mirror plane (50:50). Structure **4** was refined as an inversion twin in noncentrosymmetric space group $Pna2_1$, with a final refined component mass ratio of 52:48. The asymmetric unit contains two molecules that appear to be pseudosymmetrically related; however, parameter correlations are minimal except for those of the molybdenum atom itself. Acceptable solutions in centrosymmetric space group *Pnma* were not obtained.

See Table 1 and the Supporting Information for additional details.

Photochemical Hydrogen Generation. In a typical photolysis experiment, 2.3 mL of a $[Ru(bpy)_3]Cl_2$ stock solution (8.7×10^{-4} M in CH_3CN) was added to the vial first, followed by between 0 and 200 μL of catalyst stock solution (0.5 mM in DMF or CH_3CN). The volume was then adjusted to 2.50 mL with the same solvent. Finally, 2.50 mL of ascorbic acid stock solution (0.2 M in H_2O, pH 4.00 (NaOH)) was added, bringing the total volume to 5.00 mL. The vials were quickly transferred to the photolysis apparatus described below, sealed, and degassed with a 20% methane/80% nitrogen gas mixture.

All photochemical hydrogen evolution experiments were performed in 40 mL scintillation vials and were run in a locally constructed photolysis apparatus. The apparatus consists of a water-cooled aluminum block with 16 wells in which the reaction vials were placed. The entire assembly was mounted on an orbital shaker. Each well was individually irradiated from below with high-power Philips LumiLEDs Luxeon Star Hex royal blue (460 nm) 700 mA LEDs. The light power of each LED was set to 0.24 W using a Nova II power meter (Ophir-Spiricon LLC). Real-time pressure data from the vials were measured with Freescale semiconductor sensors (MPX4250AC6U) and recorded using Labview by National Instruments. After irradiation, 100 μL of the headspace of each vial was analyzed using a Shimadzu GC-17A gas chromatograph (5 Å molecular sieve column) to (1) confirm that hydrogen was responsible for the pressure increase and (2) quantify the amounts of hydrogen evolved using a calibration curve against the methane internal standard. Relative error is estimated to be 10%.

Electrochemical Experiments. In a typical experiment, a 0.5 mM solution of Mo complex was prepared in an electrochemical cell in either CH_3CN or DMF. Tetrabutylammonium hexafluorophosphate (TBA-PF_6) was added to bring the electrolyte concentration to 0.1 M. The cell was then fitted with a magnetic stir bar, two glassy carbon disc electrodes, and a saturated calomel electrode (SCE). The cell was then degassed under argon for 15 min. Data were collected using a scan rate of 150 mV s^{-1}. For electrocatalytic experiments, the conditions described above were employed using a hanging mercury drop working electrode where indicated. Between each cyclic voltammetry experiment, an aliquot of a 1 mM solution of trifluoroacetic acid (TFA) was added to the solution, and the electrodes were polished and washed thoroughly.

Excited-State Emission Quenching Experiments. A 10 μM solution of $[Ru(bpy)_3]Cl_2$ was prepared in either CH_3CN or DMF. One milliliter of this solution was used to prepare a solution of the desired Mo complex so that [Mo] equaled 3.0 mM; the solution was degassed with N_2. Three milliliters of the $[Ru(bpy)_3]Cl_2$ solution was added to a quartz cuvette fitted with a septum and degassed with N_2. The effect of the Mo complex on the emission of $[Ru(bpy)_3]^{2+}$ was monitored by collecting emission spectra between additions of aliquots of the Mo/$[Ru(bpy)_3]^{2+}$ solution. The spectra were taken by excitation at 460 nm with scanning from 500 to 800 nm. Both emission and excitation slits were set to 4 mm.

General Synthetic Procedure for the Molybdenum Isocyanide Complexes. ***Warning!*** *Isocyanide and benzenedithiol compounds are highly toxic and should be handled with care. n-Butyllithium is also toxic and reacts violently with water.* Molybdenum complexes were synthesized using a procedure slightly modified from that reported previously.[60] Under a nitrogen atmosphere, 100 mg (0.31 mmol) of $MoCl_4(CH_3CN)_2$, synthesized by the reaction of $MoCl_5$ and CH_3CN,[67] was suspended in 20 mL THF, resulting in a yellow−brown color. Eight equivalents of the desired isocyanide (2.5 mmol) were added to the flask, turning the suspension a reddish−brown color. In a separate flask, 0.63 mmol of the appropriate benzenedithiol was dissolved in 20 mL of THF. The solution was cooled to 0 °C, and 1.3 mmol of

dx.doi.org/10.1021/ic501440a | *Inorg. Chem.* 2014, 53, 9860−9869

n-butyllithium (1.6 M in hexanes) was added dropwise over 10 min. The solution was then allowed to warm to RT over 1 h. The solution of benzenedithiolate ligand was then slowly transferred via cannula to the flask containing the molybdenum precursor, causing the solution to turn dark immediately. The reaction was allowed to stir overnight, turning bright red. After the removal of THF using a rotary evaporator, the resulting residue was dissolved in <5 mL of CH_2Cl_2, leaving behind a white powder, which was assumed to be LiCl. The CH_2Cl_2 solution was loaded onto a silica column and eluted with a 1:1 CH_2Cl_2/diethyl ether solvent mixture. The first fraction, which is bright red, was collected. This fraction was concentrated and then loaded onto a second silica column, eluted with a 1:1 CH_2Cl_2/hexanes mixture. The first fraction, which is bright green, was discarded, and the second fraction was yellow brown. The latter fraction was collected and determined to be the desired complex. Crystals of the specific complexes are grown by slow evaporation of CH_2Cl_2.

Synthetic Procedure for [Mo(bdt)$_2$dppe] (6). ***Warning!*** *Benzene-1,2-dithiol is highly toxic and should be handled with care. n-Butyllithium is also toxic and reacts violently with water.* Complex **6** was synthesized using a modified procedure for complex **7**.[60] Under a nitrogen atmosphere, 100 mg (0.31 mmol) of $MoCl_4(CH_3CN)_2$, synthesized by the reaction of $MoCl_5$ and CH_3CN,[67] was suspended in 20 mL of THF, resulting in a yellow−brown color. Two equivalents of diphenylphosphinoethane (dppe) (0.63 mmol) were added to the flask, turning the suspension a brownish color. In a separate flask, 0.63 mmol of the appropriate benzenedithiol was dissolved in 20 mL of THF. The solution was cooled to 0 °C, and 1.3 mmol of *n*-butyllithium (1.6 M in hexanes) was added dropwise over 10 min. The solution was then allowed to warm to RT over 1 h. The solution of benzenedithiolate ligand was then slowly transferred via cannula to the flask containing the molybdenum precursor, causing the solution to turn dark immediately. The reaction was allowed to stir overnight, turning dark brown. After the removal of THF using a rotary evaporator, the resulting residue was dissolved in <5 mL of CH_2Cl_2, leaving behind a white powder, which was assumed to be LiCl. The CH_2Cl_2 solution was loaded onto a silica column and eluted with a 1:1 CH_2Cl_2/diethyl ether solvent mixture. The first fraction, which is a yellow−brown color, was collected. This fraction was concentrated and then loaded onto a second silica column, eluted with a 3:1 CH_2Cl_2/hexanes mixture. The first fraction, which is bright green, was discarded, and the second fraction was yellow brown. Crystals of **6** were grown by slow evaporation of CH_2Cl_2.

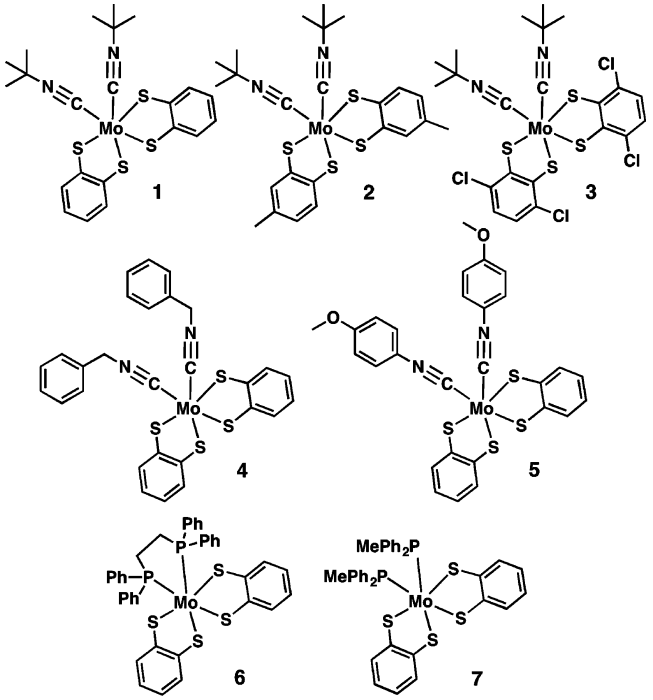

Characterization. [Mo(bdt)$_2$(*t*-BuNC)$_2$] (**1**): yield, 35 mg (20%). ^{1}H NMR (400 MHz; CD_2Cl_2): δ 8.13 (dd, J = 6.1, 3.2 Hz, 4H), 7.26 (dd, J = 6.1, 3.2 Hz, 4H), 1.58 (s, 18H). UV−vis (CH_2Cl_2) λ_{max} (ε_M) 472 (12727), 406 (12026), 241 (63737). IR (ATR): 3040 (w), 2976 (m), 2931(w), 2139 (s), 1450 (m), 1373 (s), 1186 (s), 1077 (s) cm^{-1}. Anal. Calcd for $C_{22}H_{26}MoN_2S_4$: C, 48.69; H, 4.83; N, 5.16. Found: C, 48.69; H, 4.75; N, 5.13.

[Mo(tdt)$_2$(*t*-BuNC)$_2$]·1/2CH_2Cl_2 (**2**): yield, 38 mg (21%). ^{1}H NMR (400 MHz; CD_2Cl_2): δ 7.99 (d, J = 8.2 Hz, 2H), 7.94 (s, 2H), 7.10 (d, J = 8.3 Hz, 2H), 2.44 (s, 6H), 1.57 (s, 18H). UV−vis (CH_2Cl_2) λ_{max} (ε_M) 489 (8534), 411(7377), 246 (47192). IR (ATR): 3036 (w), 2985 (w), 2923 (w), 2860(w), 2135 (s), 1587 (m), 1455 (m), 1373 (s), 1191 (s), 1084 (m) cm^{-1}. Anal. Calcd for $C_{24.5}H_{31}ClMoN_2S_4$: C, 47.99; H, 5.10; N, 4.57. Found: C, 48.27; H, 5.02; N, 4.44.

[Mo(bdt-Cl$_2$)$_2$(*t*-BuNC)$_2$] (**3**): yield, 30 mg (14%). ^{1}H NMR (400 MHz; CD_2Cl_2): δ 7.39 (s, 4H), 1.61 (s, 18H). UV−vis (CH_2Cl_2) λ_{max} (ε_M) 517 (3500) sh, 456 (5320), 408, (6155), 292 (11504) sh, 238 (62516). IR (ATR): 2963 (w), 2149 (w), 1595 (m), 1436 (m), 1391 (m), 1169 (s), 1080 (s) cm^{-1}. Anal. Calcd for $C_{22}H_{22}Cl_4MoN_2S_4$: C, 38.83; H, 3.26; N, 4.12. Found: C, 38.99; H, 3.19; N, 3.94.

[Mo(bdt)$_2$(BzNC)$_2$] (**4**): yield, 61.6 (32%). ^{1}H NMR (400 MHz; CD_2Cl_2): δ 8.15 (dd, J = 6.1, 3.2 Hz, 4H), 7.42−7.37 (m, 10H), 7.29 (dd, J = 6.1, 3.2 Hz, 4H), 5.10 (s, 4H). UV−vis (CH_2Cl_2) λ_{max} (ε_M) 478 (13510), 406 (11815), 241 (63703). IR (ATR): 3040 (w), 2950 (w), 2169 (s), 1461 (m), 1353 (m), 1233 (s), 1086 (m) cm^{-1}. Anal. Calcd for $C_{28}H_{22}MoN_2S_4$: C, 55.07; H, 3.63; N, 4.59. Found: C, 54.93; H, 3.50; N, 4.50.

[Mo(bdt)$_2$(MeOPhNC)$_2$] (**5**): yield, 14 mg (7%). ^{1}H NMR (400 MHz; CD_2Cl_2): δ 8.19 (dd, J = 6.1, 3.2 Hz, 4H), 7.46 (d, J = 9.0 Hz, 4H), 7.31 (dd, J = 6.1, 3.2 Hz, 4H), 6.96 (d, J = 9.1 Hz, 4H), 3.83 (s, 6H). UV−vis (CH_2Cl_2) λ_{max} (ε_M) 554 (9760) sh, 486 (12681), 406 (11586), 290 (32798) sh, 247 (83120). IR (ATR): 3052 (w), 2966 (w), 2123 (m), 1738 (w), 1593(s), 1500 (s), 1253 (s), 1160 (s), 1026 (m) cm^{-1}. Anal. Calcd for $C_{28}H_{22}MoN_2O_2S_4$: C, 52.33; H, 3.45; N, 4.36. Found: C, 52.32; H, 3.40; N, 4.39.

[Mo(bdt)$_2$dppe] (**6**): yield, 167 mg (69%). ^{1}H NMR (400 MHz; CD_2Cl_2): δ 8.07−8.05 (m, 4H), 7.42 (t, J = 7.1 Hz, 4H), 7.29 (t, J = 7.6 Hz, 8H), 7.20−7.13 (m, 12H), 1.69 (d, J = 15.0 Hz, 4H). ^{31}P NMR (162 MHz; CD_2Cl_2): δ 63.9. λ_{max} (ε_M) 488 (5246) sh, 435 (9268), 355 (4812), 245 (48145). IR (ATR): 3057 (w), 2933 (w), 2328 (w), 1733 (w), 1484 (m), 1431 (s), 1022 (m) cm^{-1}. Anal. Calcd for $C_{38}H_{32}MoP_2S_4$: C, 58.91; H, 4.16. Found: C, 58.72; H, 4.31.

RESULTS AND DISCUSSION

Synthesis. The molybdenum complexes studied were chosen to determine their activity as catalysts for H_2 generation and to allow evaluation of the electronic effects of both the dithiolene ligand and ancillary ligands at the same time. Using methyl- and dichloro-substituted benzenedithiolene ligands in addition to the unsubstituted form tested the influence of electron-donating and -withdrawing groups on the dithiolene backbone. The effect of the ancillary ligands was examined by employing alkyl-, benzyl-, and phenyl-substituted isocyanides as well as monodentate and bidentate phosphine ligands, while holding the dithiolene ligand constant.

Complexes **1**−**7** were synthesized from $MoCl_4(CH_3CN)_2$ in a single step and were found to be air-stable in both solid and solution states.[60] Crystals suitable for single-crystal X-ray analysis were obtained by slow evaporation of methylene chloride solutions under ambient conditions. Synthetic yields of the isocyanide complexes were typically between 7 and 30%, but the synthesis of related phosphine complexes were much better, attaining yields upward of 65%. Interestingly, we were unable to synthesize the related complex [Mo(mnt)$_2$(*t*-BuNC)$_2$] (mnt = maleonitriledithiolate) because of an apparent lack of reactivity between $MoCl_4(CH_3CN)_2$ and disodium maleonitriledithiolate, which may be due to the strongly electron-withdrawing nature of the ligand's substituents.

dx.doi.org/10.1021/ic501440a | *Inorg. Chem.* 2014, 53, 9860−9869

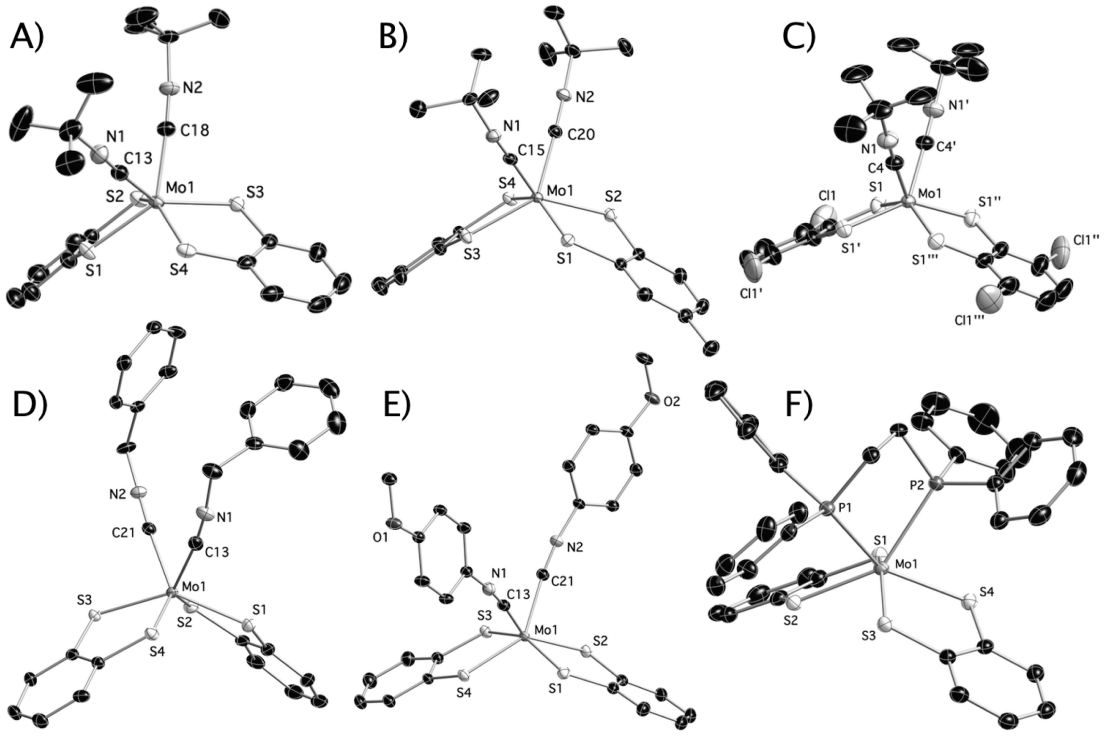

Figure 1. Molecular structures of molybdenum bis-dithiolene complexes examined as proton reduction catalysts: (A) $Mo(bdt)_2(t\text{-BuNC})_2$ (**1**), (B) $Mo(tdt)_2(t\text{-BuNC})_2$ (**2**), (C) $Mo(bdtCl_2)_2(t\text{-BuNC})_2$ (**3**), (D) $Mo(bdt)_2(BzNC)_2$ (**4**), (E) $Mo(bdt)_2(p\text{-MeOPhNC})_2$ (**5**), and (F) $Mo(bdt)_2(dppe)$ (**6**). Structures were collected at 100 K, and atoms are drawn as 50% probability ellipsoids. Hydrogen atoms are omitted for clarity.

Table 1. Selected Bond Lengths and Angles for Complexes 1−5 Compared with Those of $Mo(bdt)_2(MeNC)_2$ (8)

parameter	1	2	3	4[a]	5	8[60]
Bond Length (Å)						
Mo1−S1	2.3494(6)	2.3534(6)	2.3457(4)	2.3656(11), 2.3562(11)	2.3592(4)	2.356(2)
Mo1−S2	2.3552(7)	2.3662(6)		2.3562(11), 2.3611(11)	2.3756(4)	2.356(1)
Mo1−S3	2.3555(6)	2.3540(6)		2.3529(11), 2.3510(11)	2.3576(4)	2.358(1)
Mo1−S4	2.3554(5)	2.3626(6)		2.3604(11), 2.3582(12)	2.3610(4)	2.365(1)
$Mo-S_{avg}$	2.3539(6)	2.3591(6)	2.3457(4)	2.3577(12)	2.3634(4)	2.359(1)
Mo1−C	2.096(2)	2.087(2)	2.100(2)	2.101(4), 2.105(4)	2.0730(13)	2.093(6)
Mo1−C	2.101(2)	2.100(2)		2.104(4), 2.111(4)	2.0947(13)	2.109(5)
$Mo-C_{avg}$	2.099(3)	2.094(2)	2.100(2)	2.103(6)	2.0839(13)	2.101(6)
$C-C(dithiolene)_{avg}$	1.394(3)	1.394(3)	1.393(4)	1.394(6)	1.401(2)	1.390(6)
$C-N_{avg}$	1.147(3)	1.150(3)	1.149(3)	1.148(5)	1.1599(17)	1.146(6)
Bond Angle (deg)						
Mean $S-Mo-S_{cis}$	86.00(2)	85.99(2)	85.726(19)	84.90(4)	85.1008(12)	85.09
Mean $S-Mo-S_{trans}$	142.34(2)	141.7(2)	142.85(2)	140.11(4)	144.416(13)	140.77
C−Mo−C	79.55(9)	81.90(9)	78.99(11)	78.86(15), 79.78(16)	81.92(5)	78.9(2)
Trigonal Twist (Θ)	3.98	8.47	0.00	2.12	18.12	0.83

[a]Two Mo complexes in the asymmetric unit.

Molecular Structure. The molecular structures of complexes **1**−**6** were all found to have a slightly distorted trigonal prismatic geometry around molybdenum (Figure 1A−F), consistent with similar previously reported compounds.[60] Relevant bond lengths and angles for molybdenum isocyanide complexes (**1**−**6**) are listed in Tables 1 and 2 along with those for previously reported compounds $Mo(bdt)_2(MeNC)_2$ (**8**) and **7**,[60] respectively, for comparison. The use of noninnocent dithiolene ligands frequently leads to ambiguous assignment of oxidation states. The C−C bonds of the five-membered dithiolene chelate ring are within the expected value for an aromatic carbon−carbon bond in all structures (1.390−1.401 Å), indicating fully reduced C−S bonds; therefore, these complexes are assigned the formal oxidation state of Mo^{IV}. Mo−S bond lengths are in good agreement with those reported for **8**, ranging from 2.3197(6) to 2.3756(4) Å. Similarly, the Mo−C bonds in complexes with the isocyanide ligands showed little variation, with lengths between 2.0730(13) and 2.111(4) Å. The Mo−C−N angle was close to linear in all five structures as well (172.6−178.2°), consistent with triple bond character between the ligating carbon and adjacent nitrogen atoms. In examining the isocyanide complexes (**1**−**5**), complex **5** exhibits the greatest degree of distortion from an ideal trigonal prism with a trigonal twist[68,69] of 18.12°, as compared to 0.00−8.47° in the other structures. The phosphine complexes are similarly distorted with trigonal twists of 16.15° (**6**) and 18.52° (**7**). The largest difference between **6** and **7** is the

dx.doi.org/10.1021/ic501440a | Inorg. Chem. 2014, 53, 9860−9869

Table 2. Selected Bond Lengths and Angles for Complex 6 Compared with Those of 7

parameter	6	7[60]
Bond Length (Å)		
Mo1−S1	2.3423(6)	2.350(2)
Mo1−S2	2.3651(6)	2.351(2)
Mo1−S3	2.3197(6)	2.355(2)
Mo1−S4	2.3692(6)	2.347(2)
Mo−S_{avg}	2.3491(6)	2.351(2)
Mo1−P1	2.5148(6)	2.541(2)
Mo1−P2	2.5230(6)	2.530(2)
Mo−P_{avg}	2.5189(6)	2.536(2)
C−C(dithiolene)$_{avg}$	1.400(3)	1.392(6)
Bond Angle (deg)		
Mean S−Mo−S_{cis}	85.83(2)	85.42
Mean S−Mo−S_{trans}	141.84(2)	139.99
P1−Mo−P2	76.46(2)	87.35(6)
Trigonal Twist (Θ)	16.15	18.52

P−Mo−P angle, which results from the chelating dppe ligand in **6**, restricting this parameter to 76.46(2)°, versus the monodentate phosphine ligands in **7** with a corresponding bond angle of 87.35(6)°.

Electronic Spectra and Electrochemical Data. Although few differences are observed in the coordination sphere around molybdenum, more variations between complexes **1**−**7** can be detected in their electronic spectra and electrochemical data (Table 3 and Supporting Information, Figures S1−S6).

Table 3. Observed Electronic Transitions and Electrochemical Potentials of 1−7

complex	λ_{max}[a]	Mo^{IV}/Mo^{III}[b]	Mo^{III}/Mo^{II}[b]
1	243, 280, 406, 472	−0.79	−1.38
2	246, 281, 411, 489	−0.81	−1.38
3	238, 292, 408, 456	−0.51[c]	−1.10[c,d]
4	241, 280, 406, 478	−0.74	−1.26
5	247, 290, 406, 486, 554	−0.64	−1.03
6	245, 355, 435, 488	−0.86[c]	−1.74[c]
7	269, 361, 421, 510	−0.95	

[a]Measured in CH_2Cl_2. [b][Mo] = 0.5 mM; glassy carbon disc working and counter electrodes; reported in volts vs SCE in CH_3CN in 0.1 M tetrabutylammonium hexafluorophosphate. [c]DMF was used in place of CH_3CN for solubility. [d]Quasi-reversible couple, i_{pc}, reported.

Complexes **1**−**4** are red in color and possess two strong bands in the visible region with a shoulder of slightly lower energy. Interestingly, **5** has an additional absorption band at 554 nm, giving the complex a red−purple color. Bis-trimethylphosphine complex **6** is brown−yellow in color with spectral features in good agreement with those previously reported for **7**, displaying a single strong absorption at 435 nm with a shoulder at 488 nm.

Inductive effects from substituents on the dithiolene ligand can be seen in cyclic voltammograms of **1**−**3** (Supporting Information, Figures S7−S9). Complex **1** exhibits reversible redox events at −0.79 and −1.38 V in CH_3CN that correspond to Mo^{IV}/Mo^{III} and Mo^{III}/Mo^{II} couples, respectively. For complex **2** with its methyl substituent, the Mo^{IV}/Mo^{III} couple is shifted ca. 20 mV more negative than that of **1** with no apparent change to the Mo^{III}/Mo^{II} couple. Complex **3**, with the Cl_2bdt ligand, shows both redox couples shifted anodicly by approximately 300 mV relative to those of **1**, and the more negative reduction is quasi-reversible but similarly shifted. Complexes **4**−**7** give evidence of the effect of the auxiliary ligands (Supporting Information, Figures S10−S13). Complex **4**, with slightly less electron-donating BzNC ligands, as compared to *t*-BuNC, exhibits redox potentials only slightly more positive than those of **1**, at −0.74 and −1.26 V. The return oxidation waves for complex **4** are quasi-reversible, with two distinct waves for the more negative redox couple. This is possibly due to complex decomposition in the doubly reduced state, although it is not clear why this is observed only for **4**. Complex **5**, which showed the most deviation from **1**−**4** in both structural features and absorption spectra, shows more significantly shifted redox couples at −0.64 and −1.03 V. The redox events for complex **6** show much more separation than those for complexes **1**−**5**, with well-defined waves at −0.86 and −1.74 V. The Mo^{IV}/Mo^{III} couple for complex **7** is similar to that of **6** at −0.95 V, but it does not have a more negative wave.

Light-Driven Hydrogen Production. Initial efforts employed $[Mo(bdt)_2(t\text{-BuNC})_2]$ (**1**) as a catalyst for proton reduction in light-driven systems. Several photosensitizer/electron-donor systems were examined to fulfill the photochemical aspect of the system, with **1** serving as the catalyst. Fluorescein/5% TEA/pH 12.0, Rose Bengal/5% TEOA/pH 7.0, and $[Ir(PPy)_2(bpy)]Cl$/5% TEOA/pH 7.0 gave no detectable traces of hydrogen after 20 h of irradiation by white light LEDs (410−480 and 480−800 nm, 0.33 W). However, a system composed of **1**, $[Ru(bpy)_3]Cl_2$, and 0.1 M ascorbic acid (pH 4.0) was found to produce significant quantities of hydrogen over 24 h. Because of the strong absorption of $[Ru(bpy)_3]^{2+}$ at 450 nm, the following studies utilized blue light LEDs (max: 460 nm, 0.23 W) to optimize the light energy for the photosensitizer. Similar quantities of hydrogen were produced over a pH range of 2.6−4.0 (Supporting Information, Figure S14), but considerably less hydrogen was produced at pH > 4.0 and thus the remainder of the experiments were performed at pH 4.0.

In systems containing **1**, $[Ru(bpy)_3]Cl_2$, and ascorbic acid (pH 4.0), hydrogen was produced steadily for about 10 h before the activity slowly declined and ceased completely after 24 h. The initial rate (first 30 min of photolysis) increased linearly with increasing [**1**] (Figure 2A, inset) in the range of 4.0−16.0 μM, suggesting a first-order dependence on catalyst concentration, consistent with several previously reported systems.[18,19,24] However, when the concentration of $[Ru(bpy)_3]^{2+}$ was varied from 0.17 to 0.40 mM, little difference was seen in the initial rates (Figure 2B). Therefore, at these concentrations, the amount of catalyst is turnover-limiting. In the absence of **1**, $[Ru(bpy)_3]^{2+}$, or ascorbic acid, no hydrogen was detected after 24 h of irradiation. Furthermore, the molybdenum precursor, $MoCl_4(CH_3CN)_2$, was completely inactive toward the production of hydrogen under the same conditions. Given these results, it seems likely that the system remains homogeneous, and decomposition products of the Mo catalyst are not responsible for catalysis. To probe this further, reactions were performed with approximately 1 mL of elemental mercury present throughout the course of the experiment, giving similar results to experiments conducted without mercury (Supporting Information, Figure S15). If molybdenum nanoparticles were formed under the reducing conditions, then the formation of an amalgam would be expected along with either severely decreased catalytic activity or catalysis with very different kinetic traces.

The cause of the cessation of system activity was examined by addition of fresh solutions of **1**, $[Ru(bpy)_3]^{2+}$, and ascorbic acid after 17 h of irradiation, when much of the activity had diminished. The addition of a fresh solution of $[Ru(bpy)_3]^{2+}$

dx.doi.org/10.1021/ic501440a | Inorg. Chem. 2014, 53, 9860−9869

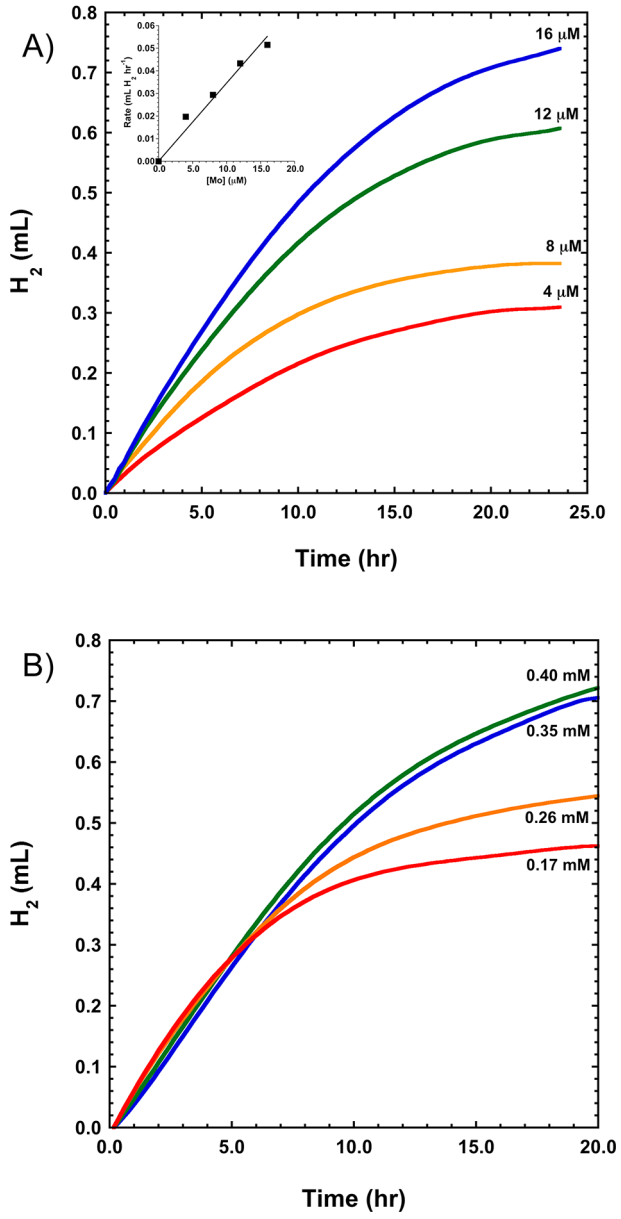

Figure 2. Light-driven hydrogen production in 1:1 water/CH_3CN, $[\text{ascorbic acid}]_0$ = 0.1 M; (A) effect of varied [**1**] at $[Ru(bpy)_3Cl_2]_0$ = 0.4 mM, inset: initial rates (mL/h) vs [**1**]; (B) effect of changing [Ru] at [**1**] = 12 mM. Relative error is 10%.

showed a slight restoration of activity, but addition of fresh catalyst had no effect. However, upon addition of both **1** and $[Ru(bpy)_3]^{2+}$, the initial activity was completely restored, indicating the decomposition of both of these components during the lengthy photolysis (Supporting Information, Figure S16). To better understand the loss of activity, electronic spectra were measured in situ, during the course of a photolysis reaction using a fiber optic probe (Supporting Information, Figure S17). Absorption bands in the visible region for $[Ru(bpy)_3]^{2+}$ and **1** significantly overlap, but the lower energy shoulder for **1** extending out to 600 nm could be identified under these conditions. A full spectrum was taken every 60 s for the first 20 min and then every hour for the remainder of the experiment. Absorptions corresponding to **1** quickly disappeared after approximately 3 min of irradiation, possibly indicative of facile reduction since H_2 production continued for several hours. The absorption band

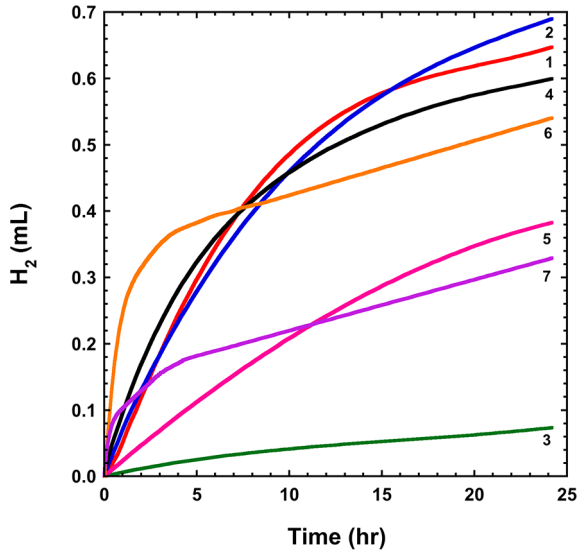

Figure 3. Performance of all molybdenum complexes as catalysts in light-driven hydrogen production. [Mo] = 12 mM, $[Ru(bpy)_3]^{2+}$ = 0.4 mM, [ascorbic acid] = 0.1 M (pH 4.0). CH_3CN/H_2O = 1:1, 15 °C, 460 nm LED light irradiation, 0.23 W.

for $[Ru(bpy)_3]^{2+}$ slowly lessened over the course of the experiment, but no other major differences were noted.

Complexes **1**−**7** were all examined as proton reduction catalysts under identical conditions, and the kinetic traces are shown in Figure 3. Complexes **1**, **2**, and **4** all have similar activity, achieving 520, 475, and 455 TON in 24 h, respectively. Both complexes **3** and **5** exhibit less activity with 100 and 260 TON, respectively. These results suggest a correlation with the redox potentials of the Mo complexes. Complexes **1**, **2**, and **4** have very similar redox potentials, whereas complexes **3** and **5** possess redox couples that are significantly more positive. This indicates that among the isocyanide complexes the greater the thermodynamic drive for hydrogen formation, the more active the catalyst. This correlates well with the observed first-order dependence on [catalyst]. The fact that no such dependence was found for the [photosensitizer] suggests that reduction of the complex is facile. The phosphine complexes display very different behavior from that of the isocyanide complexes. Complex **7**, with monodentate PPh_2Me ligands, shows modest activity, which decreases further after only a few hours, producing 135 TON after 24 h. However, its counterpart with the bidentate dppe ligand, complex **6**, has the fastest initial rate during the first 30 min of irradiation of all of the molybdenum catalysts of between 260 and 360 TON h^{-1} (Supporting Information, Figure S18), but its activity declines quickly, achieving only 402 TON after 24 h. Quantum yields calculated for each complex are <1%.

Nature of the Photochemical Step. Although light absorption by the photosensitizer initiates electron transfer to the proton reduction catalyst, this can be accomplished in one of two pathways: reductive or oxidative quenching. In the former, the absorption of light by $[Ru(bpy)_3]^{2+}$ to form $[*Ru(bpy)_3]^{2+}$ creates a strongly oxidizing electron hole, which results in oxidation of ascorbic acid and the formation of $[Ru(bpy)_3]^{+}$. Subsequent electron transfer to the Mo catalyst restores the chromophore to the Ru(II) state. In the latter, $[*Ru(bpy)_3]^{2+}$ reduces the molybdenum complex directly, yielding $[Ru(bpy)_3]^{3+}$, which irreversibly oxidizes ascorbic acid to regenerate

dx.doi.org/10.1021/ic501440a | Inorg. Chem. 2014, 53, 9860−9869

$[Ru(bpy)_3]^{2+}$. Complexes **1**−**4** and **6** were all found to quench $[*Ru(bpy)_3]^{2+}$ with rate constants near the diffusion-controlled limit (k_q= 2.12−3.5 × 10^{10} M^{-1} s^{-1}) (Supporting Information, Figures S19−S23 and Table S1). It has previously been reported that ascorbic acid quenches $[*Ru(bpy)_3]^{2+}$ with a rate constant of 1.3 × 10^8 M^{-1} s^{-1} in aqueous acetonitrile.[18] Despite roughly two orders of magnitude difference in k_q, reductive quenching is the dominant route because of the relative quencher concentrations with [ascorbic acid] approximately 10^5 greater than [Mo] (i.e., rate = k_q[Q] where Q = quencher).

Triethanolamine (TEOA) is another widely used electron donor in photochemical systems. While TEOA does not quench $[*Ru(bpy)_3]^{2+}$ reductively, it can be oxidized by $[Ru(bpy)_3]^{3+}$ to reform $[Ru(bpy)_3]^{2+}$ via the oxidative quenching pathway.[7,70,71] However, substitution of TEOA for ascorbic acid in the above photolysis systems produced no hydrogen, supporting the reductive quenching pathway. This could also be due to the more basic pH required for TEOA to operate as an electron donor (protonation of the amine makes TEOA incapable of donating an electron), making protonation of the Mo complex less favorable.

Electrochemical Studies. Complexes **1**−**6** were also examined under electrocatalytic conditions in aqueous organic solvents in the presence of organic acid to learn more about the mechanism of proton reduction. As described above, all of the isocyanide complexes displayed two well-defined redox couples in acetonitrile corresponding to Mo^{IV}/Mo^{III} and Mo^{III}/Mo^{II} with the exception of **3**, for which the more negative couple is quasi-reversible. To better correlate electrochemical and photochemical experiments, aqueous organic media were used (generally, CH_3CN/H_2O or, if solubility was a problem, DMF/H_2O). We note that in all electrochemical studies the aqueous CH_3CN systems show ∼1.6-fold more current than that of the aqueous DMF systems, which is largely due to a difference in diffusion coefficients (detailed explanation provided in Supporting Information, page S2). However, the presence of water greatly affects both the energy of the electrochemical reductions as well as their reversibility. For example, the CV for complex **1** is shown in Figure 4 in acetonitrile with various amounts of water. The Mo^{IV}/Mo^{III} reduction wave, originally centered at −0.79 V, becomes broadened with the addition of 250 μL of water and then bimodal with further additions of water, corresponding to the original species and a new one. The corresponding oxidation wave is diminished upon the introduction of water, with a new wave appearing at ca. −0.5 V. The Mo^{III}/Mo^{II} wave is originally centered at −1.4 V, but it shifts in the positive direction with each successive addition of water. At 750 μL of water, two reduction waves are visible, with the smaller one consistent with the position of the original complex, although both waves are increased in amplitude. This clearly points to the formation of a different species when water is present following initial Mo^{IV}/Mo^{III} reduction. Possible complexes include one with a protonated sulfur donor or bis(aqua)-bis(benzenedithiolato)-molybdenum(III). Electronic spectra of the starting complex in both CH_3CN and CH_3CN/H_2O environments show no change, confirming stability prior to reduction (Supporting Information, Figure S24).

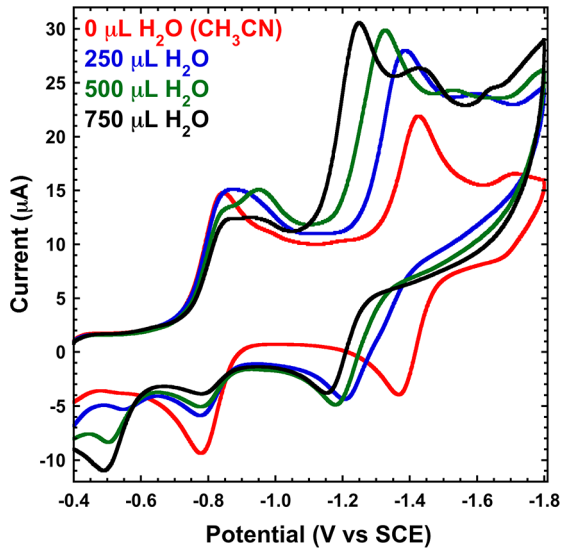

Figure 4. Effect of water on CV of **1**. Experiments were performed with glassy carbon working and auxiliary electrodes. Water was added to a 5.0 mL solution where [**1**] = 0.5 mM.

Electrocatalysis of hydrogen was studied by addition of trifluoroacetic acid (TFA) to a solution of each molybdenum complex in aqueous acetonitrile. Since proton reduction at the glassy carbon electrode was observed at potentials between −1.4 and −1.6 V, convoluting the catalytic wave corresponding to **1**, a hanging mercury drop electrode was employed because of its high overpotential for this process.[72] The effect of acid concentration on the cyclic voltammogram of **1** is shown in Figure 5. Before acid is added with the hanging mercury drop electrode, the cyclic voltammogram of the complex exhibits quasi-reversibility not seen using the glassy carbon electrode, such as that in Figure 4. The return oxidation waves have significantly less current density than that of the reduction waves, indicating that decomposition of the complex takes place in the doubly reduced state at the electrode surface, possibly due to the attraction of the sulfur atoms on the dithiolene ligand to mercury. Upon addition of 2 equiv of TFA, the reduction wave at −0.8 V appears to be mostly unchanged, shifting slightly to more positive potentials, whereas the higher energy reduction wave at −1.25 V is replaced by a new wave at −0.97 V. This wave increases in current with further addition of TFA, consistent with catalytic proton reduction. Clearly, two reduction processes are involved

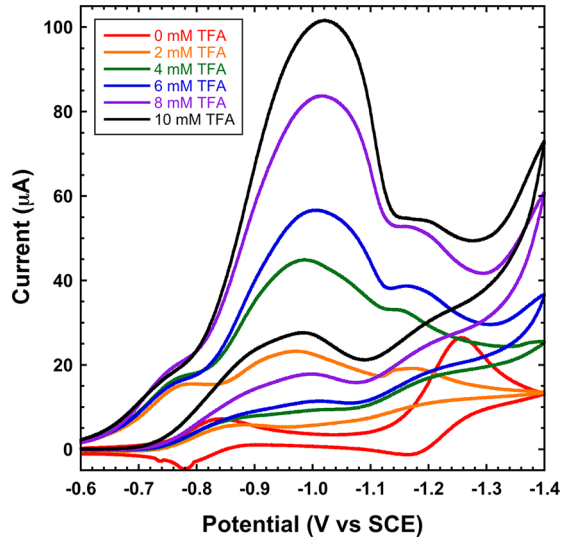

Figure 5. Electrocatalysis of **1** with a hanging mercury drop working electrode and glassy carbon auxiliary electrode. [**1**] = 0.5 mM; solvent = 9:1 CH_3CN/H_2O.

dx.doi.org/10.1021/ic501440a | Inorg. Chem. 2014, 53, 9860−9869

in the catalysis, corresponding to what has been formally described as Mo^{IV}/Mo^{III} and Mo^{III}/Mo^{II}. Given the position of the catalytic wave between the two reductions of the starting complex, it is probable that a new species forms in the presence of water after initial reduction. This may involve substitution of H_2O for the isocyanide ligand or protonation at either Mo or one of the sulfur donors, as previously postulated for cobalt bis-dithiolene complexes based on computational results.[19] This occurrence would explain the positive shift in the potential of the catalytic current relative to the second reduction potential of **1** without acid. Complexes **2** and **4** show similar behavior as that of **1**, but complexes **3** and **5** exhibit much smaller increases in current density upon addition of acid. Catalysis for complex **6** also occurs between its two reduction potentials at −1.57 V (Supporting Information, Figures S25−S31).

NMR and UV−Vis Studies. To observe species formed during catalysis of H_2 generation, $Mo(bdt)_2(t\text{-BuNC})_2$ (**1**) was studied by ^1H NMR spectroscopy. In CD_3CN, **1** shows two resonances corresponding to the bdt protons at 8.14 and 7.32 ppm and a singlet for the *t*-BuNC protons at 1.56 ppm (Figure 6A).

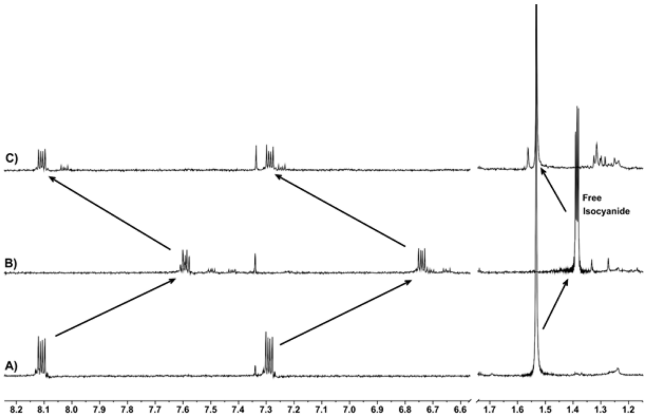

Figure 6. ^1H NMR, 400 MHz, CD_3CN, 298 K of (A) $[Mo(bdt)_2(tBuNC)_2]$ (**1**), (B) $[Mo(bdt)_2]^{2-}$, (C) $[Mo(bdt)_2]^{2-}$, and trifluoroacetic acid.

Both sets of resonances are shifted downfield relative to the free ligand (7.38 and 7.09 in CD_3CN, Supporting Information, Figure S32), indicative of coordination. Addition of D_2O or trifluoroacetic acid has no effect on the ^1H NMR spectrum of **1**. Reduction of **1** in CD_3CN by treatment with sodium amalgam under a nitrogen atmosphere for 1 h results in a color change from bright red to yellow−green. The complex thus generated is also diamagnetic, as determined by ^1H NMR resonances that are sharp and similar in number to those of **1**. The resonances for the bdt ligand in this complex are observed at 7.62 and 6.77 ppm, which are distinct from those of the free ligand, whereas the resonance corresponding to the *t*-BuNC ligand protons shifts to 1.42 ppm and appears as a triplet, indicative of free isocyanide ligand (Figure 6B and Supporting Information Figure S33). The 1:1:1 triplet of the free *t*-BuNC protons is due to ^{14}N quadrupolar coupling.[73,74] These results suggest a two-electron reduction of **1** along with dissociation of the *t*-BuNC ligands. Without the *t*-BuNC ligands, a four-coordinate Mo bis-dithiolene species, $[Mo(bdt)_2]^{2-}$, is formed. A related example of a four-coordinate Mo(II) complex, Mo(diethyldithio-carbamate)$_2$, has been structurally characterized previously.[75]

Under nitrogen and with the sodium amalgam removed, the species designated as $[Mo(bdt)_2]^{2-}$ is stable for several hours but decomposes readily in air. However, addition of TFA to the $[Mo(bdt)_2]^{2-}$ solution results in the immediate reformation of complex **1** (Figure 6C). Acetic acid and a solution of ascorbic acid at pH 4.0 are also found to regenerate the starting complex in the same way, but water at pH 7.0 has no effect. When a similar experiment was performed on a larger scale with complex **2**, hydrogen gas was detected in the flask headspace, as determined by GC analysis.[76] Slow evaporation of the solvent in this experiment leads to the formation of red crystals, which were confirmed by a unit cell analysis to be the starting complex, **2**. The formation of hydrogen by **1** was also followed by UV−vis absorption spectroscopy (Figure 7). The initial electronic

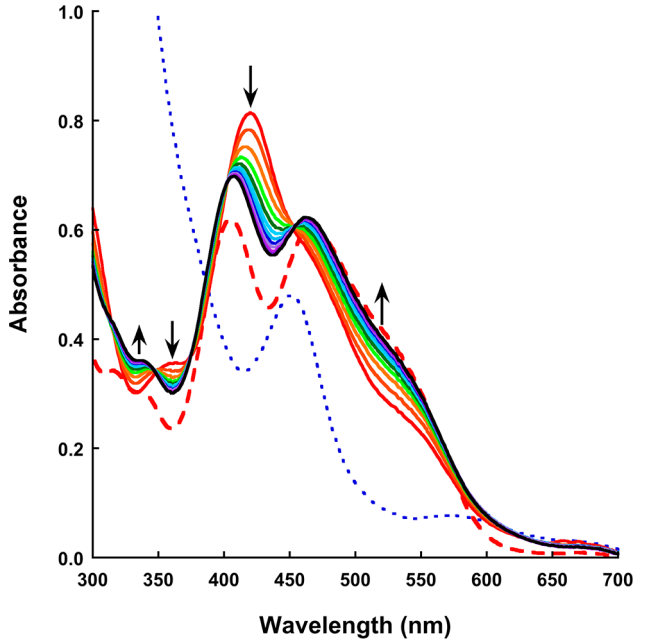

Figure 7. UV−vis absorption spectra of 40 mM complex **1** in CH_2Cl_2 (red hashed line), $[Mo(bdt)_2]^{2-}$ generated from **1** with Na/Hg (blue dotted line), and spectra taken every 10 s after addition of 70 equiv of TFA to $[Mo(bdt)_2]^{2-}$.

spectrum characteristic of **1** is shown by the red dashed line, which has strong absorptions at 405 and 468 nm and a shoulder at 535 nm. Upon reduction with Na/Hg, a yellow−green species forms that has a strong absorbance band at 451 nm with a weak shoulder at 582 nm, shown by the blue dotted line. Upon addition of 70 equiv of TFA, an intense band is observed at 420 nm that decreases over a 2 min period with the formation of the bands and shoulders characteristic of complex **1**. The isosbestic points at 312, 347, 374, 450, and 630 nm in Figure 7 indicates that there is only one observable intermediate in the conversion from $[Mo(bdt)_2]^{2-}$ to $[Mo(bdt)_2(t\text{-BuNC})_2]$ upon the addition of acid.

Mechanism of Hydrogen Formation. The observations surrounding hydrogen production with $[Mo(bdt)_2(t\text{-BuNC})_2]$ have led to a proposed mechanism as shown in Scheme 1. The steps shown in blue are based on the NMR observations described above and represent entry into the cycle. As discussed above, it is unclear from NMR studies whether the *t*-BuNC ligands dissociate after the first or second reduction. However, cyclic voltammetry experiments indicate that complex **1** undergoes two sequential reductions before catalytically generating hydrogen. The positive shift seen in the second reduction wave in the presence of water is probably due to loss of *t*-BuNC ligands, with possible coordination of water and/or protonation of the

dx.doi.org/10.1021/ic501440a | Inorg. Chem. 2014, 53, 9860−9869

Scheme 1. Proposed Mechanism of Hydrogen Formation with 1

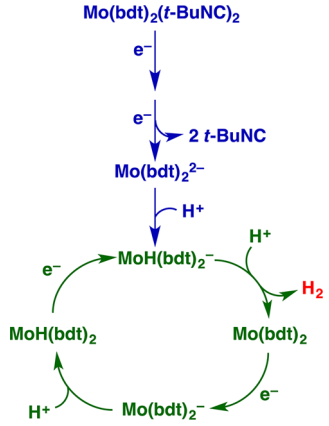

reduced complex at either the Mo ion or a sulfur donor atom. In photolysis experiments conducted with $[Ru(bpy)_3]^{2+}$ and ascorbic acid, an electron is supplied by the reduced photosensitizer, $[Ru(bpy)_3]^{+}$, to the intermediates in the catalytic cycle. The −1.33 V potential for that electron (the $[Ru(bpy)_3]^{2+}/[Ru(bpy)_3]^{+}$ couple) is sufficient to reduce the key intermediates in the cycle of Scheme 1. The lack of significant current enhancement in **3** or **5** is consistent with their poor performance as catalysts in the light-driven studies.

Whereas $[Mo(bdt)_2]^{2-}$ is moderately stable under an inert atmosphere in the presence of neutral aqueous acetonitrile, it reacts immediately in the presence of acidic protons and regenerates **1** over a period of 2 to 3 min, resulting in the evolution of H_2. Upon protonation of $[Mo(bdt)_2]^{2-}$, an intermediate is observed by UV−vis spectroscopy, which reforms into **1** over a period of about 1.5 min. This intermediate is possibly the neutral species $[Mo(bdt)_2]$, which is formed immediately after hydrogen evolution. The slow process of the conversion of $[Mo(bdt)_2]$ to **1** corresponds to the reassociation of *t*-BuNC. However, under catalytic conditions, reassociation of *t*-BuNC ligands, which are relatively dilute compared to that of free protons at pH 4.0 (~18 mM $[H^+]$ vs 24 μM [*t*-BuNC]), is unlikely. Therefore, in the catalytic cycle, the $Mo(bdt)_2$ complex generated after hydrogen evolution is probably reduced directly. Without dissociation of the *t*-BuNC ligands needed to free a coordination site, formation of a molybdenum hydride intermediate may occur after the first reduction, but it remains possible that this happens after the second reduction.

CONCLUSIONS

Homogeneous light-driven artificial photosynthetic systems employing molybdenum bis-dithiolene complexes as catalysts for proton reduction have been described. In total, seven molybdenum bis-dithiolene complexes were examined in this capacity and fully characterized. The most active catalyst, $[Mo(tdt)_2(t\text{-BuNC})_2]$, produces turnover numbers as high as 500 relative to [Mo]. Turnover frequencies were found to be highest for the diphosphine complex, $[Mo(bdt)_2(dppe)]$, and are between 260 and 360 TON h^{-1}. From ^1H NMR and electrochemical studies, a catalytic cycle is proposed that involves electron reduction and protonation steps to form H_2. Stoichiometric studies are consistent with the formation of $[Mo(bdt)_2]^{2-}$ and dissociated isocyanide ligands. In the light-driven catalytic cycle at pH 4, the protonated version of this dianion, $[MoH(bdt)_2]^{-}$, likely plays a key role. When this species encounters an acidic proton, hydrogen evolves immediately, with the resultant $[Mo(bdt)_2]$ reentering the catalytic cycle.

ASSOCIATED CONTENT

Supporting Information

X-ray crystallographic data for complexes **1**−**6** in CIF format as well as their full characterization, including NMR spectra, UV−vis absorption spectra, and IR spectra as well as experiments as mentioned in the text. This material is available free of charge via the Internet at http://pubs.acs.org.

AUTHOR INFORMATION

Corresponding Authors

*E-mail: eckenhoff@hws.edu.
*E-mail: eisenberg@chem.rochester.edu.

Notes

The authors declare no competing financial interest.

ACKNOWLEDGMENTS

Financial support from the Nation Science Foundation (CHE-1151789) is gratefully acknowledged. W.E. would like to thank the National Science Foundation for the American Competitiveness in Chemistry Postdoctoral Fellowship (CHE-1137057). Molecular structure determination by Bill Brennessel was much appreciated. Discussions relating to diffusion coefficients with Prof. Walter Bowyer were invaluable and very helpful.

REFERENCES

(1) Nocera, D. G. *Chem. Soc. Rev.* **2009**, *38*, 13.
(2) Lewis, N. S. *ChemSusChem* **2009**, *2*, 383.
(3) Teets, T. S.; Nocera, D. G. *Chem. Commun.* **2011**, *47*, 9268.
(4) Gust, D.; Moore, T. A.; Moore, A. L. *Faraday Discuss.* **2012**, *155*, 9.
(5) Lehn, J. M.; Sauvage, J. P. *Nouv. J. Chim.* **1977**, *1*, 449.
(6) Moradpour, A.; Amouyal, E.; Keller, P.; Kagan, H. B. *Nouv. J. Chim.* **1978**, *2*, 547.
(7) Kalyanasundaram, K.; Kiwi, K.; Grätzel, M. *Helv. Chim. Acta* **1978**, *61*, 2720.
(8) Keller, P.; Moradpour, A.; Amouyal, E.; Kagan, H. B. *Nouv. J. Chim.* **1980**, *4*, 377.
(9) Du, P.; Schneider, J.; Jarosz, P.; Eisenberg, R. *J. Am. Chem. Soc.* **2006**, *128*, 7726.
(10) Du, P.; Schneider, J.; Jarosz, P.; Zhang, J.; Brennessel, W. W.; Eisenberg, R. *J. Phys. Chem. B* **2007**, *111*, 6887.
(11) Du, P.; Knowles, K.; Eisenberg, R. *J. Am. Chem. Soc.* **2008**, *130*, 12576.
(12) Fihri, A.; Artero, V.; Pereira, A.; Fontecave, M. *Dalton Trans.* **2008**, 5567.
(13) Fihri, A.; Artero, V.; Razavet, M.; Baffert, C.; Leibl, W.; Fontecave, M. *Angew. Chem., Int. Ed.* **2008**, *47*, 564.
(14) Dempsey, J. L.; Brunschwig, B. S.; Winkler, J. R.; Gray, H. B. *Acc. Chem. Res.* **2009**, *42*, 1995.
(15) Probst, B.; Rodenberg, A.; Guttentag, M.; Hamm, P.; Alberto, R. *Inorg. Chem.* **2010**, *49*, 6453.
(16) Probst, B.; Guttentag, M.; Rodenberg, A.; Hamm, P.; Alberto, R. *Inorg. Chem.* **2011**, *50*, 3404.
(17) Artero, V.; Chavarot-Kerlidou, M.; Fontecave, M. *Angew. Chem., Int. Ed.* **2011**, *50*, 7238.
(18) McNamara, W. R.; Han, Z.; Alperin, P. J.; Brennessel, W. W.; Holland, P. L.; Eisenberg, R. *J. Am. Chem. Soc.* **2011**, *133*, 15368.
(19) McNamara, W. R.; Han, Z.; Yin, C. J.; Brennessel, W. W.; Holland, P. L.; Eisenberg, R. *Proc. Natl. Acad. Sci. U.S.A.* **2012**, *109*, 15594.
(20) Wilson, A. D.; Shoemaker, R. K.; Miedaner, A.; Muckerman, J. T.; DuBois, D. L.; Rakowski DuBois, M. *Proc. Natl. Acad. Sci. U.S.A.* **2007**, *104*, 6951.
(21) Appel, A. M.; Pool, D. H.; O'Hagan, M.; Shaw, W. J.; Yang, J. Y.; Rakowski DuBois, M.; DuBois, D. L.; Bullock, R. M. *ACS Catal.* **2011**, *1*, 777.

(22) Kilgore, U. J.; Roberts, J. A. S.; Pool, D. H.; Appel, A. M.; Stewart, M. P.; Rakowski DuBois, M.; Dougherty, W. G.; Kassel, W. S.; Bullock, R. M.; DuBois, D. L. *J. Am. Chem. Soc.* **2011**, *133*, 5861.
(23) Helm, M. L.; Stewart, M. P.; Bullock, R. M.; Rakowski DuBois, M.; DuBois, D. L. *Science* **2011**, *333*, 863.
(24) Han, Z.; McNamara, W. R.; Eum, M. E.; Holland, P. L.; Eisenberg, R. *Angew. Chem., Int. Ed.* **2012**, *51*, 1667.
(25) Han, Z.; Qiu, F.; Eisenberg, R.; Holland, P. L.; Krauss, T. D. *Science* **2012**, *338*, 1321.
(26) Yamada, Y.; Miyahigashi, T.; Kotani, H.; Ohkubo, K.; Fukuzumi, S. *Energy Environ. Sci.* **2012**, *5*, 6111.
(27) Ott, S.; Kritikos, M.; Åkermark, B.; Sun, L. *Angew. Chem., Int. Ed.* **2003**, *42*, 3285.
(28) Ott, S.; Borgström, M.; Kritikos, M.; Lomoth, R.; Bergquist, J.; Åkermark, B.; Hammarström, L.; Sun, L. *Inorg. Chem.* **2004**, *43*, 4683.
(29) Wang, H. Y.; Si, G.; Cao, W. N.; Wang, W. G.; Li, Z. J.; Wang, F.; Tung, C. H.; Wu, L. Z. *Chem. Commun.* **2011**, *47*, 8406.
(30) Wang, F.; Wang, W. G.; Wang, X. J.; Wang, H. Y.; Tung, C. H.; Wu, L. Z. *Angew. Chem., Int. Ed.* **2011**, *50*, 3193.
(31) Li, X.; Wang, M.; Zheng, D.; Han, K.; Dong, J.; Sun, L. *Energy Environ. Sci.* **2012**, *5*, 8220.
(32) Wang, M.; Chen, L.; Sun, L. *Energy Environ. Sci.* **2012**, 6763.
(33) Styring, S. *Faraday Discuss.* **2012**, *155*, 357.
(34) Eckenhoff, W. T.; Eisenberg, R. S. *Dalton Trans.* **2012**, *41*, 13004.
(35) Du, P.; Eisenberg, R. *Energy Environ. Sci.* **2012**, *5*, 6012.
(36) McCormick, T. M.; Han, Z.; Weinberg, D. J.; Brennessel, W. W.; Holland, P. L.; Eisenberg, R. *Inorg. Chem.* **2011**, *50*, 10660.
(37) Solis, B. H.; Hammes-Schiffer, S. *J. Am. Chem. Soc.* **2012**, *134*, 15253.
(38) Lee, C. H.; Dogutan, D. K.; Nocera, D. G. *J. Am. Chem. Soc.* **2011**, *133*, 8775.
(39) Roubelakis, M. M.; Bediako, D. K.; Dogutan, D. K.; Nocera, D. G. *Energy Environ. Sci.* **2012**, *5*, 7737.
(40) Streich, D.; Astuti, Y.; Orlandi, M.; Schwartz, L.; Lomoth, R.; Hammarström, L.; Ott, S. *Chem.—Eur. J.* **2010**, *16*, 60.
(41) Chen, L.; Wang, M.; Gloaguen, F.; Zheng, D.; Zhang, P.; Sun, L. *Inorg. Chem.* **2013**, *52*, 1798.
(42) Sobczynski, A.; Yildiz, A.; Bard, A. J.; Campion, A.; Fox, M. A.; Mallouk, T.; Webber, S. E.; White, J. M. *J. Phys. Chem.* **1988**, *92*, 2311.
(43) Sobczynski, A. *J. Catal.* **1991**, *131*, 156.
(44) Lin, L.; Kuntz, R. R. *J. Photochem. Photobiol., A* **1992**, *66*, 245.
(45) Hatay, I.; Ge, P. Y.; Vrubel, H.; Hu, X.; Girault, H. H. *Energy Environ. Sci.* **2011**, *4*, 4246.
(46) Vrubel, H.; Merki, D.; Hu, X. *Energy Environ. Sci.* **2012**, *5*, 6136.
(47) Scanlon, M. D.; Bian, X.; Vrubel, H.; Amstutz, V.; Schenk, K.; Hu, X.; Liu, B.; Girault, H. H. *Phys. Chem. Chem. Phys.* **2013**, *15*, 2847.
(48) Chen, W. F.; Iyer, S.; Iyer, S.; Sasaki, K.; Wang, C. H.; Zhu, Y.; Muckerman, J. T.; Fujita, E. *Energy Environ. Sci.* **2013**, 1818.
(49) Merki, D.; Hu, X. *Energy Environ. Sci.* **2011**, *4*, 3878.
(50) Merki, D.; Fierro, S.; Vrubel, H.; Hu, X. *Chem. Sci.* **2011**, *2*, 1262.
(51) Hinnemann, B.; Moses, P. G.; Bonde, J.; Jorgensen, K. P.; Nielsen, J. H.; Horch, S.; Chorkendorff, I.; Norskov, J. K. *J. Am. Chem. Soc.* **2005**, *127*, 5308.
(52) Bonde, J.; Moses, P. G.; Jaramillo, T. F.; Nørskov, J. K.; Chorkendorff, I. *Faraday Discuss.* **2009**, *140*, 219.
(53) Zong, X.; Yan, H.; Wu, G.; Ma, G.; Wen, F.; Wang, L.; Li, C. *J. Am. Chem. Soc.* **2008**, *130*, 7176.
(54) Zhou, W.; Yin, Z.; Du, Y.; Huang, X.; Zeng, Z.; Fan, Z.; Liu, H.; Wang, J.; Zhang, H. *Small* **2013**, *9*, 140.
(55) Appel, A. M.; DuBois, D. L.; Rakowski DuBois, M. *J. Am. Chem. Soc.* **2005**, *127*, 12717.
(56) Karunadasa, H. I.; Chang, C. J.; Long, J. R. *Nature* **2010**, *464*, 1329.
(57) Karunadasa, H. I.; Montalvo, E.; Sun, Y.; Majda, M.; Long, J. R.; Chang, C. J. *Science* **2012**, *335*, 698.
(58) Smith, A. E.; Schrauzer, G. N.; Mayweg, V. P.; Heinrich, W. *J. Am. Chem. Soc.* **1965**, *87*, 5798.
(59) Cowie, M.; Bennett, M. J. *Inorg. Chem.* **1976**, *15*, 1584.
(60) Donahue, J. P.; Goldsmith, C. R.; Nadiminti, U.; Holm, R. H. *J. Am. Chem. Soc.* **1998**, *120*, 12869.
(61) Dickinson, R. G.; Pauling, L. *J. Am. Chem. Soc.* **1923**, *45*, 1466.
(62) *APEX2*, version 2012.4-3; Bruker AXS: Madison, WI, 2012.
(63) Sheldrick, G. M. *SADABS*, version 2008/1; University of Göttingen: Göttingen, Germany, 2008.
(64) *SAINT*, version 7.68A; Bruker AXS: Madison, WI, 2009.
(65) Altomare, A.; Burla, M. C.; Camalli, M.; Cascarano, G. L.; Giacovazzo, C.; Guagliardi, A.; Moliterni, A. G. G.; Polidori, G.; Spagna, R. *J. Appl. Crystallogr.* **1999**, *32*, 115.
(66) Sheldrick, G. M. *SHELXL-97*; University of Göttingen: Göttingen, Germany, 2012.
(67) Dilworth, J. R.; Richards, R. L. *Inorg. Synth.* **1990**, *28*, 33.
(68) Stiefel, E. I.; Brown, G. F. *Inorg. Chem.* **1972**, *11*, 434.
(69) Muetterties, E. I.; Geuggenberger, L. J. *J. Am. Chem. Soc.* **1974**, *96*, 1748.
(70) Ziessel, R.; Hawecker, J.; Lehn, J. M. *Helv. Chim. Acta* **1986**, *69*, 1065.
(71) Kirch, M.; Lehn, J. M.; Sauvage, J. P. *Helv. Chim. Acta* **1979**, *62*, 1345.
(72) Felton, G. A. N.; Glass, R. S.; Lichtenberger, D. L.; Evans, D. H. *Inorg. Chem.* **2006**, *45*, 9181.
(73) Morishima, I.; Mizuno, A.; Yonezawa, T. *J. Chem. Soc. D* **1970**, 1321.
(74) Kuntz, I. D.; Schleyer, P. V. R.; Allerhand, A. *J. Chem. Phys.* **1961**, *35*, 1533.
(75) He, G. Y.; Bei, F. L.; Chen, H. Q.; Sun, X. Q. *J. Chem. Crystallogr.* **2006**, *36*, 481.
(76) This experiment was designed to follow the species present in solution and was not setup to be quantitative.